NMR Line Shape Analysis of a Multi-state Ligand Binding Mechanism in Chitosanase

Shoko Shinya
Kindai University, Nara, Japan

Mariana G. Ghinet
Université de Sherbrooke, Sherbrooke, QC, Canada

Ryszard Brzezinski
Université de Sherbrooke, Sherbrooke, QC, Canada

Kyoko Furuita
Institute for Protein Research, Osaka University, Suita, Osaka, Japan

Chojiro Kojima
Institute for Protein Research, Osaka University, Suita, Osaka, Japan

See next page for additional authors

Authors

Shoko Shinya, Mariana G. Ghinet, Ryszard Brzezinski, Kyoko Furuita, Chojiro Kojima, Sneha Shah, Evgeni Kovrigin, and Tamo Fukamizo

NMR line shape analysis of a multi-state ligand binding mechanism in chitosanase

Shoko Shinya
Department of Advanced Bioscience Kindai University Nara Japan
Institute for Protein Research Osaka University Suita Japan

Mariana G. Ghinet
Département de Biologie, Faculté des Sciences Université de Sherbrooke Sherbrooke Canada
Département de Pharmacologie, Faculté de Médecine et des Sciences de la Santé Université de Sherbrooke Sherbrooke Canada

Ryszard Brzezinski
Département de Biologie, Faculté des Sciences Université de Sherbrooke Sherbrooke Canada

Kyoko Furuita
Institute for Protein Research Osaka University Suita Japan

Chojiro Kojima
Institute for Protein Research Osaka University Suita Japan

Sneha Shah
Department of Chemistry Marquette University Milwaukee, WI

Evgenii L. Kovrigin
Department of Chemistry Marquette University Milwaukee, WI

Abstract

Chitosan interaction with chitosanase was examined through analysis of spectral line shapes in the NMR HSQC titration experiments. We established that the substrate, chitosan hexamer, binds to the enzyme through the three-state induced-fit mechanism with fast formation of the encounter complex followed by slow isomerization of the bound-state into the final conformation. Mapping of the chemical shift perturbations in two sequential steps of the mechanism highlighted involvement of the substrate-binding subsites and the hinge region in the binding reaction. Equilibrium parameters of the three-state model agreed with the overall thermodynamic dissociation constant determined by ITC. This study presented the first kinetic evidence of the induced-fit mechanism in the glycoside hydrolases.

Keywords

Electronic supplementary material

The online version of this article (doi: [10.1007/s10858-017-0109-6](10.1007/s10858-017-0109-6)) contains supplementary material, which is available to authorized users.

Introduction

Chitin, β-1,4-linked polysaccharide of *N*-acetylglucosamine (GlcNAc), is the second most abundant biomass next to cellulose (Younes and Rinaudo [2015](2015)), yet, the chitin biomass is not readily utilized due to its chemical recalcitrance. Chemical or enzymatic deacetylation of chitin produces chitosan, the amorphous and highly reactive β-1,4-linked polysaccharide of glucosamine (GlcN) (Pareek et al. [2013](2013)). The chitosan polysaccharide can be degraded by chitosanase (EC 3.2.1.132) (Monaghan et al. [1973](1973)) producing chitosan oligosaccharides, which represent the new opportunity for drug development (Raafat et al. [2008](2008); Rhoades et al. [2008](2008); Wang et al. [2007](2007)). Most chitosan polysaccharides are not completely deacetylated thus containing variable fractions of GlcNAc and GlcN. The chitosanases hydrolyze the glycosidic linkages between GlcN residues as well as the linkages between GlcN and GlcNAc (Fukamizo et al. [1994](1994)).

Substrate-binding site of the chitosanase is composed of several subsites, each of which accommodates a monomer unit of the polysaccharide substrate. Particularly, in the family GH46 chitosanase from *Streptomyces* sp. N174, CsnN174, the substrate-binding cleft features three subsites on each side of the catalytic center (Fukamizo and Brzezinski [1997](1997); Tremblay et al. [2001](2001)). According to the subsite nomenclature proposed by Davies et al. ([1997](1997)), these subsites were designated as −3, −2, −1, +1, +2, and +3, where the glycosidic bond located in between −1 and +1 subsites is cleaved by the concerted action of catalytic residues Glu22 and

Asp40 (Fukamizo and Brzezinski [1997]), and the individual subsites are positively numbered from the bond-cleavage site to the reducing end and negatively numbered to the non-reducing end. Such a long substrate-binding cleft enables the enzyme to strongly bind to the polysaccharide chain and provide for specificity of the substrate recognition as was demonstrated for the chitosan hexamer $(GlcN)_6$ (Fukamizo et al. [1995]; Fukamizo and Brzezinski [1997]).

Recently, three-dimensional structure of chitosanase OU01 from *Microbacterium* sp. (CsnOU01), whose amino acid sequence is 60% homologous to that of CsnN174, was solved by X-ray crystallography in a complex with chitosan hexamer $(GlcN)_6$ (Lyu et al. [2015]). The two chitosanases were found to have a similar fold, and the complex structure revealed interaction of $(GlcN)_6$ with the enzyme binding cleft highlighting the dominant role of the −2, −1 and +1 subsites in substrate binding and catalysis. Since most polysaccharide hydrolases have a long-extended binding cleft, oligosaccharide ligands frequently used for enzymatic analysis of the enzymes may bind to the binding cleft in multiple ways resulting in complicated binding isotherms. For example, two different binding sites were identified in CsnN174 for the chitosan trimer, $(GlcN)_3$, by fluorescence quenching experiments (Katsumi et al. [2005]).

A comparison of the chitosan-free and chitosan-bound forms of CsnOU01 reveals that the enzyme must undergo the opening conformational transition to allow for the chitosan polymer binding, while the protein structure must close upon the substrate for catalysis and open again for the product release (Lyu et al. [2015]). A similar conformational change was also reported in a family GH19 chitinase from rye seeds (Ohnuma et al. [2013]), indicating a close relationship between the mechanisms of GH46 and GH19 enzymes (Monzingo et al. [1996]). Ligand interactions coupled to conformational changes in protein structures may be sensitively resolved using nuclear magnetic resonance (NMR) line shape analysis (Agafonov et al. [2014]; Günther and Schaffhausen [2002]; Kaplan and Fraenkel [1980]; Kern et al. [1995]; Mittag et al. [2006], [2003]; Rao [1989]). In this report we analyzed NMR line shapes in titrations of CsnN174 chitosanase with substrate and product molecules to illuminate the mechanism of coupling between ligand binding and the conformational change in the protein structure.

Results

To probe the mechanism of the protein–ligand interactions in chitosanase, we conducted NMR titrations with substrate- and product-like chitosan oligomers, $(GlcN)_6$ and $(GlcN)_3$, of the catalytically incompetent E22A mutant, in which the catalytic residue Glu22 was mutated to alanine, as well as the wild-type protein (for the product). Figure [1] demonstrates a representative overlay of a series of ^1H-^{15}N HSQC spectra obtained in a titration of the E22A mutant with $(GlcN)_6$. A number of the assigned NH cross-peaks, including N23, W28, A30, G39, G43, G47, G153, T157, and D232, were significantly perturbed by addition of chitosan oligomers.
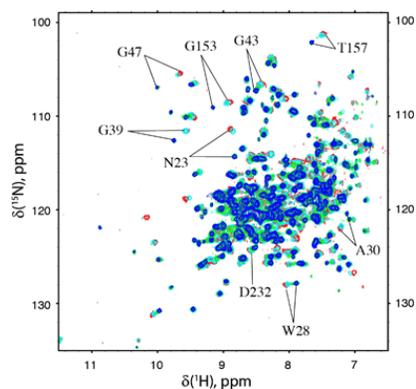
Fig. 1 ^1H-^{15}N HSQC spectra of E22A CsnN174 in the presence of different concentrations of the substrate chitosan hexaose, (GlcN)$_6$. Molar ratios of the ligand to protein concentrations are indicated by colors: 0, *red*; 0.5, *cyan*; 1.5, *green*; 3, *blue* (for clarity, only four out of seven spectra in the titration series are shown). Assigned resonances that were sufficiently resolved for line shape analysis are labeled

Figure 2 shows the backbone superimposition of the substrate-bound closed conformation of CsnOU01 (Lyu et al. 2015) with the ligand-free open form of CsnN174 (Marcotte et al. 1996). Residues with resolved NH cross-peaks sensitive to ligand binding are indicated on both closed and open structures to highlight their localization to the important functional regions of the enzyme. Specifically, the D232 and N23 are found in the "plus" chitosan binding subsites (the subsites with positive numbers) (Fukamizo and Brzezinski 1997; Tremblay et al. 2001) while G153 and T157 are residues of the "minus" subsites (subsites with the negative numbers). Residues G39 and G43 are located directly above the binding cleft and the catalytic site. The group of residues including W28, A30, G47 is relatively distant from the substrate binding site (>10 Å to the closest chitosan atom) and located in the hinge region that experiences conformational changes upon the opening-closing transition. To visualize the "hinge role" of these residues, we simulated normal modes in the ligand-free chitosanase structure. The Supplementary Movie 1 demonstrates the lowest non-trivial normal mode that interconverts the open and closed enzyme conformations. Notable that residues N23 and G39 are the nearest neighbors of the catalytic residues E22 and D40 thus capable of reporting on rearrangement of the active site into the conformation resembling the catalytic state of the chitosanase.
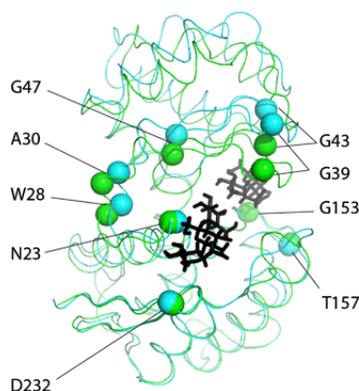

Fig. 2 Flexibility of chitosanase and distribution of the resolved NMR probes. Free CsnN174 (PDB: 1CHK), *cyan tube*; D43A CsnOU01 complexed with (GlcN)$_6$ (PDB: 4QWP), *green tube* and *black sticks*, respectively. Protein structures are aligned through the C-terminal domain (residues 121–236). NH groups of residues

with chemical shifts perturbed by ligand binding are shown as *spheres* (residue numbers correspond to the CsnN174 sequence)

Titration of the E22A CsnN174 with the substrate, chitosan hexamer, revealed a common line shape evolution pattern: the initial resonance was shifting and disappearing upon titration progress while a peak of the ligand-bound state appeared in the new location (Fig. 1). This pattern may be caused by four possible molecular mechanisms (Kovrigin 2012): (A) pre-existing dimerization equilibrium when the dimer is incapable of ligand binding, (B) dimerization of the bound state to form a dimer that cannot dissociate the ligands, (C) binding of two ligand molecules to different binding sites, and (D) the ligand binding followed by isomerization to a tightly bound complex (the induced fit mechanism) (Fig. 3).
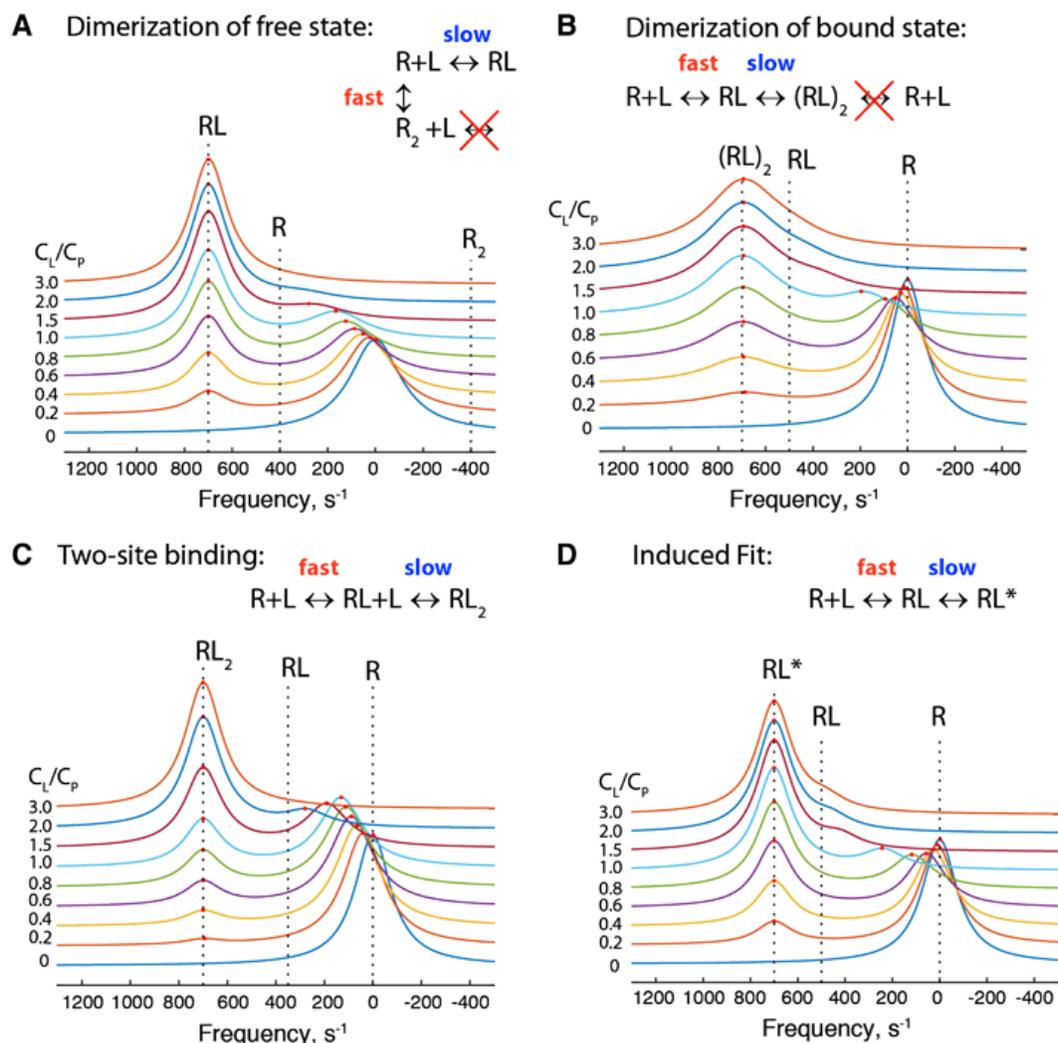

Fig. 3 Simulations of the three-state mechanisms that may be responsible for spectral patterns observed in the chitosanase titrations with the substrate $(GlcN)_6$. The exchange regime on NMR time scale is indicated for each kinetic step. Frequencies of individual species are shown with *vertical dashed lines*. For detailed kinetic and thermodynamics simulation parameters see Materials and Methods. The model names according to LineShapeKin Simulation: **a** U-R2; **b** U-R2L2; **c** B; **d** U-RL. One-dimensional spectra

were simulated for the range of ligand-to-protein molar ratios, C_L/C_P (indicated next to the corresponding traces), and displaced vertically for clarity

It is unlikely, that two substrate molecules may be bound at the same time to chitosanase because the long-chain oligosaccharide such as $(GlcN)_6$ is known to fully engage the binding cleft (Lyu et al. 2015)—eliminating two-binding site mechanism Fig. 3c. The dimerization of chitosanase in ligand-free or bound forms (Fig. 3a, b) is expected to approximately double the rotational correlation time of the enzyme leading to the increased observed line widths (see Supplementary section "Estimation of the monomer and dimer line widths"). Dimerization of the bound state in the slow exchange regime (Fig. 3b) results in the resolved resonance of the dimer, therefore this mechanism may be readily detected through the line width measurements of the free and bound states. The mean proton line widths of the ligand-free and substrate-bound chitosanase samples were 30 and 29 Hz, respectively, with the standard deviation of 5 Hz (Supplementary section "Measurement of proton line widths"). Since the bound form of the enzyme did not demonstrate significantly increased line width, the mechanism with dimerization of the bound form (Fig. 3b) was also eliminated.

We tested relative ability of the two remaining mechanisms in Fig. 3, panels a and d, to account for the experimental data by fitting of both mathematical models to a series of 1D spectral datasets of resonances of W28, G39, G153, and T157 resolved in proton dimension, and G43 and T157 resolved in the nitrogen dimension using IDAP NMR line shape analysis software (Kovrigin 2012). Results in the Fig. 4 demonstrate that both mathematical models are capable of reproducing general features of the experimental datasets. The induced fit model (U-RL, Fig. 3d) was capable of fitting all datasets in one global fitting session to a single set of kinetic and thermodynamic constants (Fig. 4, top row). We obtained values of equilibrium dissociation constants of 42 μM and isomerization constant of 3.9 with the reverse rate constants of 30,000 and 9 s^{-1} for the dissociation and isomerization, respectively.
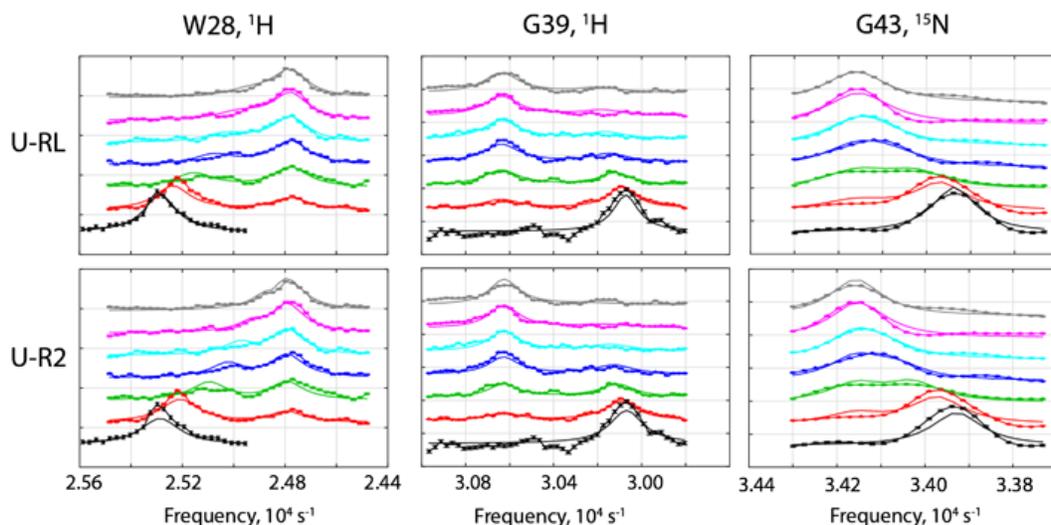

Fig. 4 Representative NMR line shapes from the titration E22A CsnN174 chitosanase with $(GlcN)_6$ fit using the IDAP software with two alternative models: the induced-fit mechanism (U-RL, *top* row) and the protein dimerization in a free state with ligand binding to a monomer (U-R2, *bottom* row). The 1D spectral slices

correspond to ligand to protein molar ratios of 0 (*black*), 0.5 (*red*), 1 (*green*), 1.5 (*blue*), 2 (cyan), 3 (magenta), 4 (*gray*). The U-RL model fit the data for six residues in one global fitting session to a single set of kinetic and thermodynamic constants. The U-R2 model was not capable of fitting all data to a single set of global parameters; the presented graphs are from individual fitting sessions for each residue

The model with chitosanase dimers incapable of binding a ligand (U-R2, Fig. 3a) did not successfully fit all datasets in one session. The reason to that became obvious after fitting each dataset individually—the model required vastly different values of equilibrium and rate constants for different residues. The major challenge for the U-R2 model was to satisfy a narrow line width of the initial resonance despite the increased line width of the dimer relative to the monomer. The optimization algorithm achieved the desired narrow line widths by shifting the population of dimer-monomer equilibrium predominantly to the monomer (extremely low dimerization constants). However, to be able to account for significant peak shifts observed during titrations, the U-R2 model required nonsensical values of the chemical shift of a dimer (600–15,000 ppm) and unrealistically fast dimer dissociation rate constants of 10^9–10^{11} s^{-1} to maintain the fast-exchange regime—indicating that the real molecular mechanism is unlikely to resemble the U-R2 model in Fig. 3a.

To further improve our confidence that U-R2 model was not a correct choice, we analyzed variation of the chemical shifts and line widths upon dilution of the ligand-free chitosanase sample. Dilution of the sample with the monomer–dimer equilibrium in fast exchange will shift the averaged peak towards the monomer and result in a narrower line width. Supplementary Fig. 2 and 3 reveal insignificant changes in line widths and chemical shifts of the signals supporting rejection of U-R2 model as a possible mechanism for chitosanase interaction with its substrate.

Considering the "closed" conformation of the substrate-bound chitosanase observed in the crystal (Fig. 2, green tube), we may assume that in solution the conformation of CsnN174 tightly bound with (GlcN)$_6$ is also similarly closed. Titration with the product, (GlcN)$_3$, (Fig. 5) revealed that chemical shifts of the hinge residues in the substrate- and product-saturated CsnN174 are nearly identical. Similarity of the magnetic environments of the hinge residues in the end states of both titrations indicates that the product is also capable of inducing the closed enzyme conformation (albeit at much greater solution concentrations).
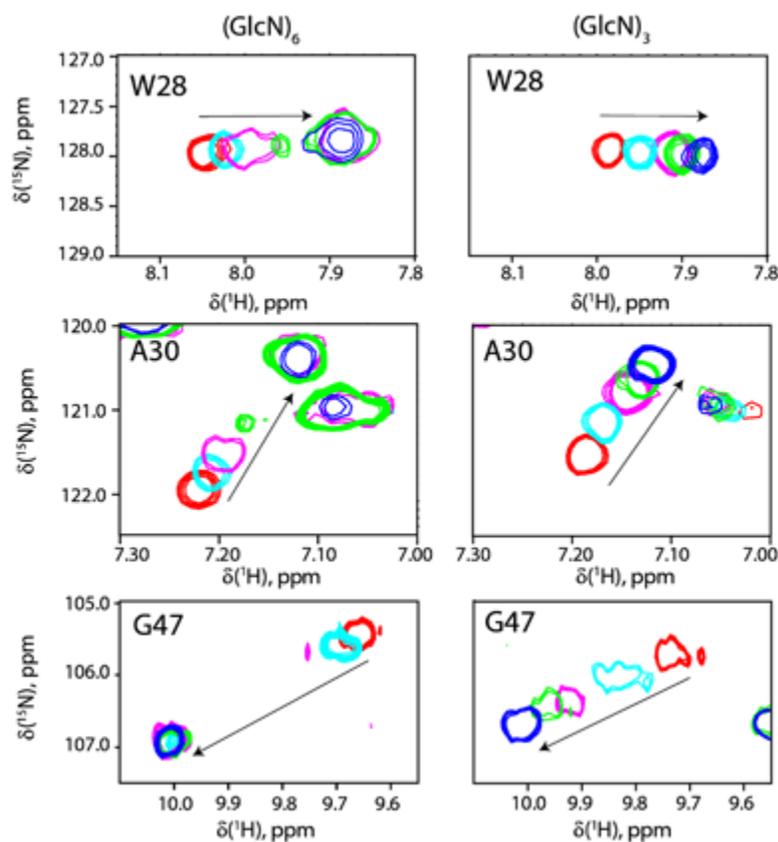
Fig. 5 Chemical shift perturbations of the hinge residues in titrations of E22A CsnN174 with the substrate, $(GlcN)_6$, and the product, $(GlcN)_3$. Molar ligand-to-protein ratio (from *red* to *blue*): 0, 0.5, 1, 1.5, and 3 for $(GlcN)_6$, *left column*; 0, 2, 5, 10, and 50 for $(GlcN)_3$, *right column*

Using Isothermal Titration Calorimetry (ITC) we measured the equilibrium dissociation constants for the product and substrate interaction with the enzyme to be 1120 ± 70 and 22 ± 3 µM for $(GlcN)_3$ and $(GlcN)_6$, respectively (Supplementary Fig. 4; Supplementary Table 1). Assuming similar diffusion-limited on-rate constants, the off-rate constant of the product is expected to be, at least, one order of magnitude faster than that of the substrate leading to the fast-exchange regime in NMR spectra. This is in agreement with the averaged shifting peak pattern observed in chitosanase-product titration (Fig. 5, right column).

The exchange-averaged line shapes such as in $(GlcN)_3$ titration in Fig. 5 cannot provide enough information for unambiguous determination of the product interaction mechanism (Kovrigin 2012). One of the means to reduce the conformational exchange rate constants without altering chemical structure of the protein is deuteration, which results in increased energy barriers for the hydrogen-bond making and breaking (Kohen 2003; Kovrigin and Loria 2006; Krantz et al. 2000). To obtain the protein sample with some hydrogen bonds replaced with the deuterium bonds, we expressed CsnN174 on the deuterated medium and partially back-exchanged the protein to protonated water to allow for the amide NH signal detection. Due to different solvent accessibility, some of the amide groups (for example, G47) remained deuterated resulting in the slower conformational exchange regime in the protein structure.

Figure 6 demonstrates the line shapes of the hinge residues in the perdeuterated CsnN174 (wild-type—in this experiment) recorded in the (GlcN)$_3$ titration. The fast-exchange pattern observed in Fig. 5 (right column) is replaced with the fast-exchange disappearing peak accompanied by a growing slow-exchange resonance of the bound state resembling the substrate titration line shapes in Fig. 5 (left column). We observe that the second step in the chitosan interaction with CsnN174 is significantly deccelerated with deuteration revealing (at least) the three-state binding mechanism. Since the residues W28 and A30 are localized to the hinge region of chitosanase, we may conclude that binding of the product is likely to proceed through a similar induced-fit steps as binding of the substrate. The "hooked" peak shift of W28 indicates the second product molecule binding to the closing enzyme, which is in accord with our ITC results (Supplementary Table 1) and the literature reports (Katsumi et al. 2005).
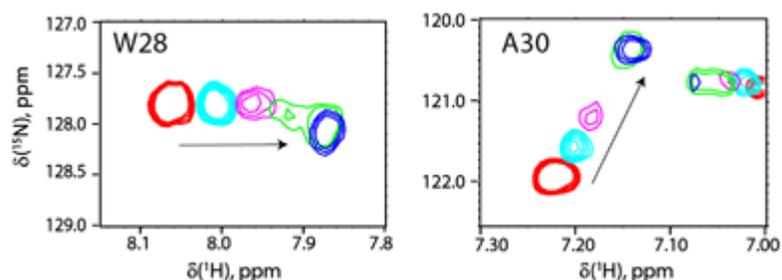

Fig. 6 Multi-state peak evolution in the deuterated and partially back-exchanged wild-type CsnN174 sample titrated with the chitosan trimer, (GlcN)$_3$. Molar ligand:protein ratio (from *red* to *blue*): 0, 4, 10, 20, and 50

To allow for a more accurate determination of quantitative parameters of the substrate binding mechanism in CsnN174, we performed fitting of the experimental NMR HSQC spectra of the titration of protonated E22A chitosanase with (GlcN)$_6$ using the two-dimensional NMR line shape fitting software TITAN (Waudby et al. 2016). Two-dimensional line shape analysis allows for fitting of peaks that appear in crowded regions such as N23, A30, and G47, for which the one-dimensional line shape extraction used in IDAP was not reliable. The total of nine amide NH peaks (residues N23, W28, A30, G39, G43, G47, G153, T157, and D232) were simultaneously fit with the induced-fit model optimizing the residue-specific chemical shifts and line widths along with the common equilibrium and rate constants for the association and isomerization steps. Quality of fitting of experimental HSQC datasets with the induced-fit model in TITAN is demonstrated in Supplementary Fig. 5. The peak positions and apparent relaxation rates of the initial ligand-free state were determined from fitting the single dataset corresponding to free CsnN174. The peak positions of the encounter complex, RL, and the final bound state, RL*, were determined from simultaneous fitting of all titration points. Chemical shift differences between the R, RL, and RL* states calculated with the Eq. 1 are plotted in Supplementary Fig. 6 while Supplementary Fig. 7 summarizes the best-fit apparent relaxation rate constants and supplementary Table 2 gives the global equilibrium and kinetic parameters. Similar quantitative analyses of the product titrations of protonated CsnN174 in the fast-exchange regime resulted in unstable best-fit results. In the deuterated sample, the degree of back-exchange was difficult to control thus rendering best-fit parameters qualitative. Therefore, in this paper, we focused

on the chitosanase interaction with the substrate leaving the product interactions for future work.

Discussion

Consideration of the "open" and "closed" crystal structures of CsnOU01 (Fig. 2) along with kinetic and thermodynamic studies led to the proposed induced-fit interaction mechanism (Lyu et al. 2015). Site-resolved analysis of chemical shift perturbations may be informative on relative roles of different residues in separate steps of enzyme-substrate interactions. Figure 7 visualizes chemical shift perturbations reported in Supplementary Fig. 6 for each of the two kinetic steps as well as the overall chemical shift perturbation due to the full process. As might have been anticipated, the residues N23, G153, and T157 show significant perturbation in the ligand-binding step (Fig. 7a) as they are directly implicated in binding interactions with the chitosan substrate. G153 and T157 are less perturbed in the second step—readjustment of the enzyme-substrate complex to the tightly bound species (Fig. 7b).
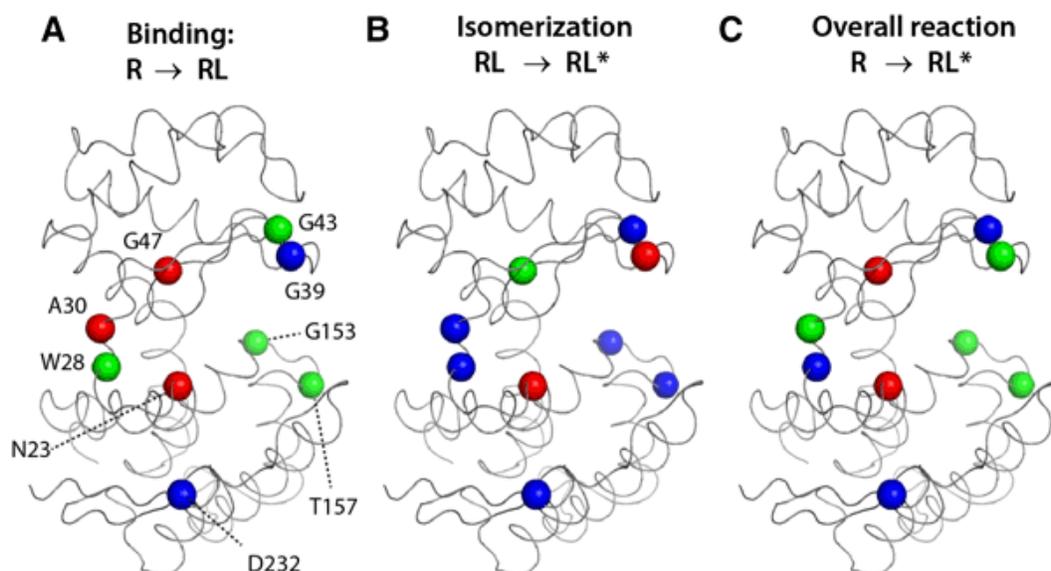

Fig. 7 Mapping of chemical shift perturbations in the two kinetic steps of the mechanism of substrate-enzyme interaction in CsnN174. The NH groups (*spheres*) were colored according to the magnitude of the chemical shift perturbations: *blue*, below the lower threshold in Supplementary Fig. 6; *green*, between the lower and upper thresholds; and *red*, above the upper threshold

It is remarkable that hinge residues W28, A30, and G47 are perturbed to a greater degree in the fast initial step of the mechanism than in the second, slow step (cf. Fig. 7 panels a and b). One may propose two possible explanations for this observation. The chitosan is a highly charged molecule; therefore, formation of the encounter complex may be sensed far beyond the binding cleft of CsnN174. In this scenario, the chemical shift perturbations in the hinge due to the substrate binding could exceed ones induced by a subsequent conformational change due to closing of the enzyme in the slow step (Supplementary Fig. 8a). The alternative explanation of the relatively greater perturbation of the hinge in the first step assumes that closing of the

enzyme actually happens during the fast phase of the binding process. In this case, slow rearrangement in the second phase must be of much smaller scale—occurring mostly around the residues of N23 and G39 located in the immediate neighborhood of the catalytic Glu22 and Asp40 (Supplementary Fig. 6, Fig. 7b). Essentially, the second explanation implies a four-state mechanism with formation of the open first-encounter complex followed by fast hinge closing followed by a slow conformational readjustment (Supplementary Fig. 8b). The first two transitions would occur in the fast-exchange regime, therefore not resolvable in our analysis.

One may note that the off-rate constant for the substrate-binding step was determined to be quite large—on the order of 20,000 s^{-1} (Supplementary Table 2). In the three-state induced-fit mechanism (Supplementary Fig. 8a), it would describe dissociation of a weak initial encounter complex, which is expected to be labile. The equilibrium dissociation constant and the off-rate constant determined by line shape fitting corresponded to the second-order association rate constant of ca. 5×10^8 M^{-1} s^{-1}, which is in a diffusion limit. Considering positively charged chitosan substrate and the negatively charged enzyme binding site, the on-rate is likely to be accelerated by their mutual electrostatic attraction.

In simulations of fast-exchange mechanisms published previously, one of us demonstrated that the sequential fast-exchange transitions between three states produce line shapes that are difficult to discern from a simpler two-state model (Kovrigin 2012). However, it was remarkable that the observed line shape evolution should have appeared in a *significantly slower* exchange regime than might be expected from the exchange rate constants of the individual steps (Fig. 4 in (Kovrigin 2012)). Therefore, the four-state model in Supplementary Fig. 8b would require unrealistically fast kinetics in binding and closing steps to still yield the overall reverse rate constant of 20,000 s^{-1} in the fast phase of the process. Based on these considerations, we chose the three-state model with fast formation of a weak open encounter complex followed by slow closing of the enzyme into a catalytically competent state to be the most likely chitosanase mechanism (Supplementary Fig. 8a).

The apparent dissociation constant of the substrate-enzyme complex determined in our ITC measurement, $K_{d,ITC} = 22 \pm 3$ µM, may be compared with NMR-derived parameters of the three-state mechanism considering a relationship of the overall dissociation constant of the multistep mechanism to equilibrium constants of the individual steps: $Kd,overall=Kd,RL/Kiso$. Substitution of the best-fit parameters yields overall K_d of 12 ± 4 µM, which is close but not identical to the ITC result, likely, due to systematic biases in ITC and NMR analyses as well as possible underestimation of the best-fit uncertainties.

From the relatively slow kinetics of the induced-fit step, we can anticipate closing of the initial enzyme-substrate complex to be the rate-limiting step of the chitosan hydrolysis. Small magnitude of the isomerization equilibrium constant between open and closed states of chitosanase (Supplementary Table 2) indicates that the two protein conformations are nearly isoenergetic, separated by ΔG^0 of only 2.8 kJ/mol. With such a weak preference for the closed state, the slow kinetics of interconversion might serve as a "lock" ensuring that the catalytically competent enzyme-substrate complex is sufficiently long-lived to allow for the effective

chitosan cleavage. The product release following the catalytic reaction is expected to be fast as judged by the fast-exchange kinetics of the product titration series (Fig. 5) and low product binding affinity (Supplementary Table 1).

In conclusion, we revealed the induced-fit mechanism in the substrate-enzyme interaction in chitosanase CsnN174, which is the first kinetic demonstration for the multi-step substrate binding in the glycoside hydrolases. Our study emphasizes the power of the NMR line shape analysis to illuminate the distinct functional roles of different structural elements in the enzyme-substrate and product recognition. Complementing the NMR line shape analysis with NMR spin relaxation measurements and molecular dynamics simulations in the future work may enable building of a highly resolved structural picture of ligand interactions and internal conformational dynamics in chitosanase.

Methods

Vectors and bacterial strains

The pFDES vector (Sanssouci et al. 2011) was used for the expression of wild type and mutant CsnN174. The *csn*N174 gene (wild type or bearing the mutation E22A) (Boucher et al. 1995) was cloned as a *Hin*dIII-*Not*I fragment into pFDES digested with the same restriction enzymes. *Streptomyces lividans* TK24 *ΔcsnR* (formerly *Δ2657h*) (Dubeau et al. 2009) was used as recipient for the recombinant plasmids.

Protein expression and purification

Enzymes, wild-type CsnN174 and E22A CsnN174, were produced as extracellular proteins by the heterologous host *S. lividans* TK24 *ΔcsnR*. Spores of *S. lividans ΔcsnR* harboring the recombinant plasmids were inoculated into tryptic soy broth (TSB) medium with 50 µg ml^{-1} kanamycin. Cultures were incubated 48 h at 30 °C with shaking (230 rpm min^{-1}). Mycelium was recovered by low speed centrifugation and inoculated in a modified M14 medium (Page et al. 1996) composed of 1 g l^{-1} KH$_2$PO$_4$, 5 g l^{-1} K$_2$HPO$_4$, 0.68% N^{15}H$_4$Cl, 1 g l^{-1} K$_2$SO$_4$, 1 ml l^{-1} of trace elements solution (2 mg ml^{-1} CoCl$_2$·7H$_2$O, 5 mg ml^{-1} FeSO$_4$·7H$_2$O, 1.6 mg ml^{-1} MnSO$_4$·H$_2$O and 1.4 mg ml^{-1} ZnSO$_4$·7H$_2$O), pH 6.9. Before use, 0.3 g l^{-1} MgSO$_4$ and 0.3 g l^{-1} CaCl$_2$ were added to the M14 medium. 10 g l^{-1} mannitol (for single isotope labelling) or 10 g l^{-1} glucose C$_6$–C^{13} (for double isotope labelling) were used as carbon sources. For obtaining the deuterated CsnN174, 99% ^{2}H$_2$O (Cambridge Isotope Laboratories) was used instead of H$_2$O. Cultures were incubated for 96 h at 30 °C with shaking (230 rpm min^{-1}). Mycelial pellet was separated from the supernatant by low speed centrifugation and discarded. Chitosanases were purified following a simple two-step procedure, using the ÄKTA explorer system (GE Healthcare). The culture supernatants were adjusted to pH 4.5 with 1 M acetic acid and loaded on a HiTrap SP-Sepharose (GE Healthcare Bio-Sciences, Baie d'Urfé, QC, Canada) column equilibrated with sodium acetate 50 mM buffer pH 4.5. These conditions are favourable for the heterologous chitosanase attachment on the resin, but not for the attachment of the endogenous one (CsnA encoded by gene *sco0677*) (Ghinet et al. 2010), produced in a very small amount by the host

strain. After washing the unbound proteins with 2 CV (column volumes) of sodium acetate 50 mM pH 4.5, a second washing step was performed with 2 CV of sodium acetate 50 mM pH 4.5 plus 50 mM NaCl. CsnN174 was eluted with sodium acetate 50mM pH 4.5 plus 0.2 M NaCl and the chosen fractions were dialysed against a solution of 1 mM $MgCl_2$ then loaded on a Hydroxyapatite Fast Flow (Calbiochem, Darmstadt, Germany) column pre-equilibrated with 1 mM $MgCl_2$. CsnN174 was eluted with 70 mM $MgCl_2$ and the fractions containing the purified protein were dialysed against 50 mM sodium acetate buffer pH 5.5. The purity of the enzyme preparations was evaluated by SDS–PAGE (Laemmli [1970](#)). Protein concentration was determined by the method of Bradford (Bradford [1976](#)) using bovine serum albumin as a standard. Protein concentration of purified chitosanases was determined by ultraviolet absorbance (280 nm) using molar extinction coefficients of 30,300 M^{-1} cm^{-1}.

Isothermal titration calorimetry

E22A CsnN174 solution (48.2–130 µM) in 50 mM sodium phosphate buffer (pH 7.0) were degassed and their concentrations were determined. Chitosan oligomers $(GlcN)_3$ and $(GlcN)_6$ were dissolved in the same buffer (1–50 mM), and the solution pH was adjusted to 7.0 by NaOH. Then the ligand solution was degassed and loaded into a syringe, while the protein solution (0.2028 ml) was loaded into the sample cell after confirming the solution pH 7.0. Calorimetric titration was performed with an iTC200 system (Microcal Northampton, MA) at 25 °C. Aliquots (1.0–2.0 µl) of the ligand solution were added to the sample cell with a stirring speed of 1000 rpm. Titrations were completed after 18–38 injections. The ITC data were analyzed with the MicroCal Origin (GE) as well as in-house IDAP software (available from Dr. Kovrigin). Statistical hypothesis testing was performed utilizing Akaike's information criterion (Akaike [1973](#), [1981](#); Motulsky and Christopoulos [2004](#)). Best-fit parameter error ranges and parameter correlations were determined through Monte-Carlo analysis.

Nuclear magnetic resonance spectroscopy

NMR samples contained 0.2–0.5 mM protein in 50 mM sodium acetate buffer pH 5.5 (90% H_2O/10% D_2O). All NMR spectra were acquired at 300 K using a Bruker AVANCE 500, 800 or 950 spectrometer controlled with TopSpin 3.0 software and equipped with a triple-resonance pulsed-field-gradient cryoprobe head. [1]H chemical shifts were referenced to HDO (4.64 ppm at 30 °C) relative to TSP. [15]N and ^{13}C chemical shifts were indirectly calibrated from each gyromagnetic ratio (Wishart et al. [1995](#)).

Sequential assignments were performed using ^{15}N/^{13}C-labelled CsnN174 and E22A CsnN174 from two-dimensional ^{1}H-^{15}N HSQC and three-dimensional HNCACB, CBCA(CO)NH, HNCA, HNCACO, HNCO, and HNCOCA experiments (Kay et al. [1990](#)). All spectra were processed using NMRPipe software (Delaglio et al. [1995](#)) and were analyzed using Sparky software (Goddard and Kneller).

TROSY-based ^{1}H-^{15}N HSQC spectrum and three dimensional spectra, TROSY-HNCO, TROSY-HNCACO, TROSY-HNCACB, and TROSY-CBCA(CO)NH were measured using ^{2}H/^{15}N/^{13}C-labelled CsnN174. The assignment data were deposited in Biological Magnetic Resonance Data Bank under Accession Nos. 11493 and 11494.

Two-dimensional ^{1}H-^{15}N HSQC spectra were recorded for 0.09–0.1 mM CsnN174 in 50 mM sodium acetate buffer pH 5.5 (90% H$_2$O/10%D$_2$O), in the presence of various concentrations of the ligands. Peak assignment of the bound states in (GlcN)$_3$ titration was done by careful tracing the shifts of fast-exchange averaged peaks through the titration. The longer chain chitosan oligomer (GlcN)$_6$ displayed slow-exchange behavior precluding direct assignment transfer. However, comparison of (GlcN)$_3$ and (GlcN)$_6$ titrations revealed that final bound state resonances positions were relatively independent of the ligand type, which allowed to assign the bound states of CsnN174 with (GlcN)$_6$ by comparison with (GlcN)$_3$ saturated spectra (Supplementary Fig. 9). Averaged chemical shift differences, $\Delta\delta av$, induced by oligosaccharide binding or isomerization plotted in Supplementary Fig. 6 were calculated according to the Eq. 1 (Grzesiek et al. 1996):

$$\Delta\delta_{av} = \sqrt{\frac{(\Delta\delta_{HN})^2 + (\frac{\Delta\delta_N}{5})^2}{2}} \quad (1)$$

where $\Delta\delta HN$ and $\Delta\delta N$ stands for chemical shifts difference between the first and the last point in the titrations for ^{1}H and ^{15}N, respectively. The uncertainty of the chemical shift difference is calculated according to standard error propagation rules (Taylor 1997).

NMR line shape simulations

Simulations of the NMR line shape mechanisms in Fig. 3 were performed with LineShapeKin Simulation 4 (http://lineshapekin.net/#LineShapeKinSimulation411) using the parameters outlined below. The full width at half-height of the peaks (FWHH) of 180 s^{-1} was used as a typical line width in chitosanase spectra to represent monomeric species; this value was doubled to obtain the dimer FWHH—according to estimates in Supplementary Information, section "Estimation of the monomer and dimer line widths".

(A) Pre-existing dimerization equilibrium when the dimer is incapable of ligand binding:

U-R2 model; equilibrium association constant K$_A$=10,000; equilibrium dimerization constant K$_B$=1000; dissociation rate constant k$_{2A}$ = 5 s^{-1}; dimer dissociation rate constant k$_{2B}$ = 2000 s^{-1}; frequencies of R, R$_2$, and RL were 400, −400, and 700 s^{-1}, respectively;

(B) Dimerization of the protein–ligand complex such that ligand cannot dissociate from the dimer:

U_R2L2 model; equilibrium association constant K$_A$ = 5000; equilibrium dimerization constant K$_B$ = 100,000; dissociation rate constant k$_{2A}$ = 2000 s^{-1}; dimer dissociation rate constant k$_{2B}$ = 5 s^{-1}; frequencies of R, RL, and (RL)$_2$ were 0, 500, and 700 s^{-1}, respectively;

(C) Binding of two ligand molecules with distinctly different off-rates:

B model; microscopic equilibrium association constants for binding the first ligand K_{A1} = 10,000 (assumed identical for both sites); microscopic equilibrium association constant for binding the second ligand molecule, K_{A2} = 100,000; microscopic dissociation rate constants of the first and second ligands were k_{2A1} = 1000 s^{-1}, k_{2A2} = 1 s^{-1}, respectively; frequencies of R, RL and RL$_2$ were 0, 350, and 700 s^{-1}, respectively;

(D) Induced fit mechanism:

U-RL model; equilibrium association constant K_A = 10,000; equilibrium isomerization constant K_B = 10; dissociation rate constant k_{2A} = 3000 s^{-1}; reverse isomerization rate constant k_{2B} = 1 s^{-1}; frequencies of R, RL and RL* were 0, 500, and 700 s^{-1}, respectively.

NMR line shape fitting

Fitting of the NMR titration data was performed using the in-house software IDAP (available from Dr. Evgenii Kovrigin) and TITAN (Waudby et al. 2016). IDAP was utilized to fit alternative mechanisms with U-RL and U-R2 models. TITAN was used without modifications to fit the two-dimensional NMR data with the "Induced Fit" model (U-RL), but the U-R2 model was not included in the available TITAN version. The uncertainties of the best-fit parameters in TITAN were determined using bootstrap error analysis with 100 re-sampling runs.

Normal mode analysis

Normal Mode Analysis was performed using the elNemo web interface to the Elastic Network Model (Suhre and Sanejouand 2004; Tirion 1996) accessible at URL: http://www.sciences.univ-nantes.fr/elnemo/. The input to the elNemo server consisted of the one chain of ligand-free chitosanase extracted from PDBID 1CHK structure. The lowest frequency non-trivial normal mode (#7) that approximated the conformational transition between open and closed states of the chitosanase was exported to the MPEG video format and provided as the Supplementary Movie 1.

Notes

Acknowledgements

Compliance with ethical standards

Conflict of interest

The authors declare that they have no conflict of interest.

References

Agafonov RV, Wilson C, Otten R, Buosi V, Kern D (2014) Energetic dissection of Gleevec's selectivity toward human tyrosine kinases. Nat Struct Mol Biol 21:848–853. doi: 10.1038/nsmb.2891

Akaike H (1973) Information theory and an extension of the maximum likelihood principle. In: Petrov BN, Csaki BF (eds) Second International Symposium on Information Theory. Academiai Kiado, Budapest, pp 267–281

Akaike H (1981) Likelihood of a model and information criteria. J Econometrics 16:3–14

Boucher I, Fukamizo T, Honda Y, Willick GE, Neugebauer WA, Brzezinski R (1995) Site-directed mutagenesis of evolutionary conserved carboxylic amino acids in the chitosanase from streptomyces sp. N174 reveals two residues essential for catalysis. J Biol Chem 270:31077–31082

Bradford MM (1976) A rapid and sensitive method for the quantitation of microgram quantities of protein utilizing the principle of protein-dye binding. Anal Biochem 72:248–254

Davies GJ, Wilson KS, Henrissat B (1997) Nomenclature for sugar-binding subsites in glycosyl hydrolases. Biochem J 321(Pt 2):557–559

Delaglio F, Grzesiek S, Vuister GW, Zhu G, Pfeifer J, Bax A (1995) NMRPipe: a multidimensional spectral processing system based on UNIX pipes. J Biomol NMR 6:277–293

Dubeau MP, Ghinet MG, Jacques PE, Clermont N, Beaulieu C, Brzezinski R (2009) Cytosine deaminase as a negative selection marker for gene disruption and replacement in the genus Streptomyces and other actinobacteria. Appl Environ Microbiol 75:1211–1214. doi: 10.1128/AEM.02139-08

Fukamizo T, Brzezinski R (1997) Chitosanase from Streptomyces sp. strain N174: a comparative review of its structure and function. Biochem Cell Biol 75:687–696

Fukamizo T, Ohkawa T, Ikeda Y, Goto S (1994) Specificity of chitosanase from Bacillus pumilus. Biochim Biophys Acta 1205:183–188

Fukamizo T, Honda Y, Goto S, Boucher I, Brzezinski R (1995) Reaction mechanism of chitosanase from Streptomyces sp. N174. Biochem J 311(Pt 2):377–383

Ghinet MG, Roy S, Poulin-Laprade D, Lacombe-Harvey ME, Morosoli R, Brzezinski R (2010) Chitosanase from Streptomyces coelicolor A3(2): biochemical properties and role in protection against antibacterial effect of chitosan. Biochem Cell Biol 88:907–916. doi: 10.1139/O10-109

Goddard TD, Kneller DG (1997) SPARKY 3; http://www.cgl.ucsf.edu/home/sparky/. University of California, San Francisco

Grzesiek S, Stahl SJ, Wingfield PT, Bax A (1996) The CD4 determinant for downregulation by HIV-1 Nef directly binds to Nef. Mapping of the Nef binding surface by NMR. BioChemistry 35:10256–10261. doi: 10.1021/bi9611164

Günther UL, Schaffhausen B (2002) NMRKIN: Simulating line shapes from two-dimensional spectra of proteins upon ligand binding. J Biomol NMR 22:201–209

Kaplan JI, Fraenkel G (1980) NMR of chemically exchanging systems. Academic Press, Cambridge

Katsumi T, Lacombe-Harvey ME, Tremblay H, Brzezinski R, Fukamizo T (2005) Role of acidic amino acid residues in chitooligosaccharide-binding to *Streptomyces* sp. N174 chitosanase. Biochem Biophys Res Commun 338:1839–1844. doi: 10.1016/j.bbrc.2005.10.157

Kay LE, Ikura M, Tschudin R, Bax A (1990) Three-dimensional triple-resonance NMR spectroscopy of isotopically enriched proteins. J Magn Reson 213:423–441. doi: 10.1016/j.jmr.2011.09.004

Kern D, Kern G, Scherer G, Fischer G, Drakenberg T (1995) Kinetic analysis of cyclophilin-catalyzed prolyl cis/trans isomerization by dynamic NMR spectroscopy. BioChemistry 34:13594–13602

Kohen A (2003) Kinetic isotope effects as probes for hydrogen tunneling, coupled motion and dynamics contributions to enzyme catalysis. Prog Reac Kinet Mec 28:119–156

Kovrigin EL (2012) NMR line shapes and multi-state binding equilibria. J Biomol NMR 53:257–270. doi: 10.1007/s10858-012-9636-3

Kovrigin EL, Loria JP (2006) Characterization of the transition state of functional enzyme dynamics. JACS 128:7724–7725

Krantz BA, Moran LB, Kentsis A, Sosnick TR (2000) D/H amide kinetic isotope effects reveal when hydrogen bonds form during protein folding. Nat Struct Biol 7:62–71

Laemmli UK (1970) Cleavage of structural proteins during the assembly of the head of bacteriophage T4. Nature 227:680–685

Lyu QQ et al. (2015) Structural and biochemical insights into the degradation mechanism of chitosan by chitosanase OU01. Biochim Biophys Acta 1850:1953–1961 doi: 10.1016/j.bbagen.2015.06.011

Marcotte EM, Monzingo AF, Ernst SR, Brzezinski R, Robertus JD (1996) X-ray structure of an anti-fungal chitosanase from *Streptomyces* N174. Nat Struct Biol 3:155–162

Mittag T, Schaffhausen B, Gunther UL (2003) Direct observation of protein-ligand interaction kinetics. BioChemistry 42:11128–11136

Mittag T, Franzoni L, Cavazzini D, Schaffhausen B, Rossi GL, Gunther UL (2006) Retinol modulates site-specific mobility of apo-cellular retinol-binding protein to promote ligand binding. J Am Chem Soc 128:9844–9848

Monaghan RL, Eveleigh DE, Tewari RP, Reese ET (1973) Chitosanase, a novel enzyme. Nature 245:78–80

Monzingo AF, Marcotte EM, Hart PJ, Robertus JD (1996) Chitinases, chitosanases, and lysozymes can be divided into procaryotic and eucaryotic families sharing a conserved core. Nat Struct Biol 3:133–140

Motulsky H, Christopoulos A (2004) Fitting models to biological data using linear and nonlinear regression: a practical guide to curve fitting. 1st edn. Oxford University Press, USA. http://www.graphpad.com/manuals/prism4/RegressionBook.pdf

Ohnuma T, Umemoto N, Kondo K, Numata T, Fukamizo T (2013) Complete subsite mapping of a "loopful" GH19 chitinase from rye seeds based on its crystal structure. FEBS Lett 587:2691–2697. doi: 10.1016/j.febslet.2013.07.008

Page N, Kluepfel D, Shareck F, Morosoli R (1996) Effect of signal peptide alterations and replacement on export of xylanase A in *Streptomyces lividans*. Appl Environ Microbiol 62:109–114

Pareek N, Vivekanand V, Agarwal P, Saroj S, Singh RP (2013) Bioconversion to chitosan: a two stage process employing chitin deacetylase from *Penicillium oxalicum* SAEM-51. Carbohydr Polym 96:417–425. doi: 10.1016/j.carbpol.2013.04.005

Raafat D, von Bargen K, Haas A, Sahl H-G (2008) Insights into the mode of action of chitosan as an antibacterial compound. Appl Environ Microbiol 74:3764–3773 doi: 10.1128/aem.00453-08

Rao BDN (1989) Nuclear magnetic resonance line-shape analysis and determination of exchange rates. Methods Enzymol 176:279–311

Rhoades J et al (2008) Oligosaccharide-mediated inhibition of the adhesion of pathogenic *Escherichia coli* strains to human gut epithelial cells in vitro. J Food Prot 71:2272–2277

Sanssouci E, Lerat S, Grondin G, Shareck F, Beaulieu C (2011) tdd8: a TerD domain-encoding gene involved in Streptomyces coelicolor differentiation. Antonie Van Leeuwenhoek 100:385–398. doi: 10.1007/s10482-011-9593-y

Suhre K, Sanejouand YH (2004) ElNemo: a normal mode web server for protein movement analysis and the generation of templates for molecular replacement. Nucl Acid Res 32:W610–614 doi: 10.1093/nar/gkh368

Taylor JR (1997) An introduction to error analysis. 2nd edn. University Science Books, California

Tirion MM (1996) Large amplitude elastic motions in proteins from a single-parameter, atomic analysis. Phys Rev Lett 77:1905–1908

Tremblay H, Yamaguchi T, Fukamizo T, Brzezinski R (2001) Mechanism of chitosanase-oligosaccharide interaction: subsite structure of Streptomyces sp. N174 chitosanase the role of Asp57 carboxylate. J Biochem 130:679–686

Wang Y, Zhou P, Yu J, Pan X, Wang P, Lan W, Tao S (2007) Antimicrobial effect of chitooligosaccharides produced by chitosanase from Pseudomonas CUY8. Asia Pac J Clin Nutr 16(Suppl 1):174–177

Waudby CA, Ramos A, Cabrita LD, Christodoulou J (2016) Two-dimensional NMR lineshape analysis. Sci Rep 6:8 doi: 10.1038/srep24826

Wishart DS, Bigam CG, Holm A, Hodges RS, Sykes BD (1995) 1H, 13C and 15N random coil NMR chemical shifts of the common amino acids. I. Investigations of nearest-neighbor effects. J Biomol NMR 5:67–81

Younes I, Rinaudo M (2015) Chitin and chitosan preparation from marine sources. Structure, properties and applications. Mar Drugs 13:1133–1174. doi: 10.3390/md13031133

Supplementary material

[10858_2017_109_MOESM1_ESM.docx](#) (3.4 mb)
Supplementary material 1 (DOCX 3496 KB)
[10858_2017_109_MOESM2_ESM.mpg](#) (336 kb)
Supplementary material 2 (MPG 335 KB)